



Published in final edited form as:

Nat Med. 2001 June ; 7(6): 673–679.

Classification and diagnostic prediction of cancers using gene expression profiling and artificial neural networks

Javed Khan^{1,2}, Jun S. Wei¹, Markus Ringnér^{1,3}, Lao H. Saal¹, Marc Ladanyi⁴, Frank Westermann⁵, Frank Berthold⁶, Manfred Schwab⁵, Cristina R. Antonescu⁴, Carsten Peterson³, and Paul S. Meltzer¹

¹Cancer Genetics Branch, National Human Genome Research Institute, National Institutes of Health, Bethesda, Maryland, USA

²Pediatric Oncology Branch, Advanced Technology Center, National Cancer Institute, Gaithersburg, Maryland, USA

³Complex Systems Division, Department of Theoretical Physics, Lund University, Lund, Sweden

⁴Department of Pathology, Memorial Sloan-Kettering Cancer Center, New York, New York, USA

⁵Department of Cytogenetics, German Cancer Research Center, Heidelberg, Germany

⁶Department of Pediatrics, Klinik für Kinderheilkunde der Universität zu Köln, Köln, Germany

Abstract

The purpose of this study was to develop a method of classifying cancers to specific diagnostic categories based on their gene expression signatures using artificial neural networks (ANNs). We trained the ANNs using the small, round blue-cell tumors (SRBCTs) as a model. These cancers belong to four distinct diagnostic categories and often present diagnostic dilemmas in clinical practice. The ANNs correctly classified all samples and identified the genes most relevant to the classification. Expression of several of these genes has been reported in SRBCTs, but most have not been associated with these cancers. To test the ability of the trained ANN models to recognize SRBCTs, we analyzed additional blinded samples that were not previously used for the training procedure, and correctly classified them in all cases. This study demonstrates the potential applications of these methods for tumor diagnosis and the identification of candidate targets for therapy.

The small, round blue cell tumors (SRBCTs) of childhood, which include neuroblastoma (NB), rhabdomyosarcoma (RMS), non-Hodgkin lymphoma (NHL) and the Ewing family of tumors (EWS), are so named because of their similar appearance on routine histology¹. However, accurate diagnosis of SRBCTs is essential because the treatment options, responses to therapy and prognoses vary widely depending on the diagnosis. As their name implies, these cancers are difficult to distinguish by light microscopy, and currently no single test can precisely distinguish these cancers. In clinical practice, several techniques are used for diagnosis, including immunohistochemistry², cytogenetics, interphase fluorescence *in situ* hybridization³ and reverse transcription (RT)-PCR (ref. 4). Immunohistochemistry allows the detection of protein expression, but it can only examine one protein at a time. Molecular techniques such as RT-PCR are used increasingly for diagnostic confirmation following the discovery of tumor-specific translocations such as *EWS-FLII*; t(11;22)(q24;q12) in EWS, and the *PAX3-FKHR*; t(2;13)(q35;q14) in alveolar rhabdomyosarcoma¹ (ARMS). However, molecular markers do not always provide a definitive diagnosis, as on occasion there is failure

Correspondence should be addressed to J.K. or P.S.M.; email: khanjav@mail.nih.gov or pmeltzer@nhgri.nih.gov.

J.K., J.S.W. and M.R. contributed equally to this study.

to detect the classical translocations, due to either technical difficulties or the presence of variant translocations.

Gene-expression profiling using cDNA microarrays permits a simultaneous analysis of multiple markers, and has been used to categorize cancers into subgroups^{5–8}. However, despite the many statistical techniques to analyze gene-expression data, none so far has been rigorously tested for their ability to accurately distinguish cancers belonging to several diagnostic categories.

Artificial neural networks (ANNs) are computer-based algorithms which are modeled on the structure and behavior of neurons in the human brain and can be trained to recognize and categorize complex patterns⁹. Pattern recognition is achieved by adjusting parameters of the ANN by a process of error minimization through learning from experience. They can be calibrated using any type of input data, such as gene-expression levels generated by cDNA microarrays, and the output can be grouped into any given number of categories. ANNs have been recently applied to clinical problems such as diagnosing myocardial infarcts¹⁰ and arrhythmias from electrocardiograms¹¹ and interpreting radiographs and magnetic resonance images^{12,13}. Here we applied ANNs to decipher gene-expression signatures of SRBCTs and used them for diagnostic classification.

Calibration and validation of the ANN models

To calibrate ANN models to recognize cancers in each of the four SRBCT categories, we used gene-expression data from cDNA microarrays containing 6567 genes. The 63 training samples (see Supplemental Table A) included both tumor biopsy material (13 EWS and 10 RMS) and cell lines (10 EWS, 10 RMS, 12 NB and 8 Burkitt lymphomas (BL; a subset of NHL)). For two samples, ST486 (BL-C2 and C4) and GICAN (NB-C2 and C7), we performed two independent microarray experiments to test the reproducibility of the experiments and these were subsequently treated as separate samples. Filtering for a minimal level of expression reduced the number of genes to 2308 (Fig. 1a). Principal component analysis (PCA) further reduced the dimensionality, and we found that using the 10 dominant PCA components per sample as inputs and four outputs (EWS, RMS, NB or BL) produced well-calibrated ANN models. These 10 dominant components contained 63% of the variance in the data matrix. The remaining PCA components contained variance unrelated to separating the four cancers. The three-fold cross-validation procedure (see Methods) produced a total of 3750 ANN models, and the training and validation was successful (Fig. 1b). In addition, there was no sign of ‘over-training’ of the models, as would be shown by a rise in the summed square error for the validation set with increasing training iterations or ‘epochs’ (Fig. 1b). Using these ANN models, all of the 63 training samples were correctly assigned/classified to their respective categories, having received the highest committee vote (average output) for that category.

Optimization of genes utilized for classification

We next determined the contribution of each gene to the classification by the ANN models by measuring the sensitivity of the classification to a change in the expression level of each gene, using the 3750 previously calibrated models (see Supplementary Methods). In this way, we ranked the genes according to their significance for the classification. We then determined the classification error rate using increasing numbers of these ranked genes. The classification error rate minimized to 0% at 96 genes (Fig. 1c). The 10 dominant PCA components for these 96 genes contained 79% of the variance in the data matrix. Using only these 96 genes, we recalibrated the ANN models (Fig. 1a) and again correctly classified all 63 samples (Fig. 2). Moreover, multidimensional scaling (MDS) analysis⁵ using these 96 genes clearly separated the four cancer types (Fig. 3a). The top 96 discriminators represented 93 unique genes (Fig. 3b), as *IGF2* was represented by three independent clones and *MYC* by two. Of the 96, 13 were

anonymous expressed sequence tags (ESTs); 16 genes were specifically expressed in EWS, 20 in RMS, 15 in NB and 10 in BL. Twelve genes were good discriminators on the basis of lack of expression in BL and variable expression in the other three types. One gene (EST; Clone ID 295985) discriminated EWS from other cancer types by its lack of expression in this cancer. The remainder of the genes was expressed in two of the four cancer types. To our knowledge, of the 61 genes that were specifically expressed in a cancer type, 41 have not been previously reported as associated with these diseases.

Diagnostic classification and hierarchical clustering

We then tested the diagnostic classification capabilities of these ANN models on a set of 25 blinded test samples. A sample is classified to a diagnostic category if it receives the highest vote for that category and because this classifier has only four possible outputs, all samples will be classified to one of the four categories. We therefore established a diagnostic classification method based on a statistical cutoff to enable us to reject a diagnosis of a sample classified to a given category. If a sample falls outside the 95th percentile of the probability distribution of distances between samples and their ideal output (for example, for EWS it is $EWS = 1, RMS = NB = BL = 0$), its diagnosis is rejected (see Methods).

The test samples contained both tumors (5 EWS, 5 RMS and 4 NB) and cell lines (1 EWS, 2 NB and 3 BL). We also tested the ability of these models to reject a diagnosis on 5 non-SRBCTs (consisting of 2 normal muscle tissues (Tests 9 and 13) and 3 cell lines including an undifferentiated sarcoma (Test 5), osteosarcoma (Test 3) and a prostate carcinoma (Test 11)). Using the 3750 ANN models calibrated with the 96 genes, we correctly classified 100% of the 20 SRBCT tests (Table 1 & Fig. 2) as well as all 63 training samples (see Supplemental Table A). Three of these samples, Test 10, Test 20 and EWS-T13 were correctly assigned to their categories (RMS, EWS and EWS respectively), having received the highest vote for their respective categories. However, their distance from a perfect vote was greater than the expected 95th percentile distance (Fig. 2); therefore, we could not confidently diagnose them by this criterion. All of the five non-SRBCT samples were excluded from any of the four diagnostic categories, since they fell outside the 95th percentiles. Using these criteria for all 88 samples, the sensitivity of the ANN models for diagnostic classification was 93% for EWS, 96% for RMS and 100% for both NB and BL. The specificity was 100% for all four diagnostic categories. Also, hierarchical clustering¹⁴ using the 96 genes, identified from the ANN models, correctly clustered all 20 of the test samples (Fig. 3c). Moreover, the two pairs of samples that were derived from two cell lines, BL-C2 and C4 (ST486) and NB-C2 and C7 (GICAN), were adjacent to one another in the same cluster.

Expression of FGFR4 on SRBCT tissue array

To confirm the effectiveness of the ANN models to identify genes that show preferential high expression in specific cancer types at the protein level, we performed immunohistochemistry on SRBCT tissue arrays for the expression of fibroblast growth factor receptor 4 (FGFR4). This tyrosine kinase receptor is expressed during myogenesis¹⁵ but not in adult muscle, and is of interest because of its potential role in tumor growth¹⁶ and in prevention of terminal differentiation in muscle¹⁷. Moderate to strong cytoplasmic immunostaining for FGFR4 was seen in all 26 RMSs tested (17 alveolar, 9 embryonal). We also observed generally weaker staining in EWS and NHL in agreement with the microarray results, except for one case of anaplastic large cell lymphoma that was strongly positive (data not shown).

Discussion

Tumors are currently diagnosed by histology and immunohistochemistry based on their morphology and protein expression, respectively. However, poorly differentiated cancers can

be difficult to diagnose by routine histopathology. In addition, the histological appearance of a tumor cannot reveal the underlying genetic aberrations or biological processes that contribute to the malignant process. Here we developed a method of diagnostic classification of cancers from their gene-expression signatures and identified the genes that contributed to this classification.

We used the SRBCTs of childhood as a model because these cancers occasionally present diagnostic difficulties. For example, Ewing sarcoma is diagnosed by immunohistochemical evidence of MIC2 expression¹⁸ and lack of expression of the leukocyte common antigen CD45 (excluding lymphoma), muscle-specific actin or myogenin (excluding RMS)¹⁹. However, reliance on detection of MIC2 alone can lead to incorrect diagnosis as MIC2 expression occurs occasionally in other tumor types including RMS and NHL (ref. 1).

Monitoring global gene-expression levels by cDNA microarrays provides an additional tool for elucidating tumor biology as well as the potential for molecular diagnostic classification of cancer^{5-8,20-22}. Currently, classification and clustering tools using gene-expression data have not been rigorously tested for diagnostic classification of more than two categories. Other approaches that share the parametric nature of ANNs and have been utilized to classify gene-expression profiles include Support Vector Machines²³. Thus far, these other methods have not been fully explored to extract the genes or features that are most important for the classification performance and which also will be of interest to cancer biologists²⁴.

Here we have approached this problem using ANN-based models. We calibrated ANN models on the expression profiles of 63 SRBCTs of 4 diagnostic categories. Due to the limited amount of training data and the high performance achieved, we limited our analysis to linear (that is, no hidden layers) ANN models. Although other linear methods may perform as well, our method can easily accommodate nonlinear features of expression data if required. To compensate for heterogeneity within the tumor samples (which contain both malignant and stromal cells) and for possible artifacts due to growth of cell lines in tissue culture, we used both tumor samples ($n = 23$) and cell lines ($n = 40$). Data from these samples is complementary, because tumor tissue, though complex, provides a gene-expression pattern representative of tumor growth *in vivo*, while cell lines contain a uniform malignant population without stromal contamination. Despite using only NB cell lines for calibrating the ANN models, all four NB tumors among the test samples were correctly diagnosed with high confidence. This not only demonstrates the high similarity of NB cell lines to the tumors of origin, but also validates the use of cell lines for ANN calibration. The calibrated ANN models accurately classified all 63 training SRBCTs and showed no evidence of over-training, demonstrating the robustness of this technique.

A potential difficulty with ANN-based pattern recognition models is elucidating causal links from the output to the original input data. To solve this problem and to identify the most significant genes, we calculated the sensitivity of the classification to a change in the expression level of each gene. We produced a list of genes ranked by their significance to the classification. Using this list, we established that the top 96 genes reduced the misclassifications to zero, which opens the potential for cost effective fabrication of SRBCT subarrays in diagnostic use. When we tested the ANN models calibrated using the 96 genes on 25 blinded samples, we were able to correctly classify all 20 samples of SRBCTs and reject the 5 non-SRBCTs. This supports the potential use of these methods as an adjunct to routine histological diagnosis.

Although ANN analysis leads to identification of genes specific for a cancer with implications for biology and therapy, a strength of this method is that it does not require genes to be exclusively associated with a single cancer type. This allows for classification based on complex gene-expression patterns. For example, the top 96 discriminating genes included not

only those that had high (61) or low levels (12 BL and 1 EWS) of expression in one particular cancer, but also genes that were differentially expressed in two diagnostic categories as compared to the remaining two. Of the 16 genes highly expressed only in EWS, two (*MIC2* and *GYG2*) have been previously described^{18,25}. *MIC2* immunostaining is currently used to diagnose EWS; however we find that although *MIC2* detects EWS with high sensitivity, it alone cannot be used to discriminate EWS as it was also expressed in several RMSs.

Our method identifies genes related to tumor histogenesis, but includes genes that may not normally be expressed in the corresponding mature tissue. Of the 14 genes that have not yet been reported to be highly expressed in EWS, 4 (*TUBB5*, *ANXA1*, *NOE1* and *GSTM5*)^{26–29} were neural-specific genes—lending more credence to the proposed neural histogenesis of EWS (ref. 30). Twenty genes were highly expressed only in RMS, including eight specific for muscle tissue and five (*FGFR4*, *IGF2*, *MYL4*, *ITGA7* and *IGFBP5*)^{15,31–34} related to myogenesis. Among the latter, *IGF2*, *MYL4* and *IGFBP5* expression has been reported in RMS (refs. 35–36), and only *ITGA7* and *IGFBP5* were found to be expressed in our two normal muscle samples. Of the genes specifically expressed in a cancer type, 41 have not been previously reported, including 7 ESTs with no current known function. All of these warrant further study and might provide new insights into the biology of these cancers. For example, *FGFR4*, a tyrosine kinase receptor that is expressed during myogenesis and prevents terminal differentiation in myocytes^{15,17}, was found to be highly expressed only in RMS and not in normal muscle. The relatively strong differential expression of *FGFR4* in RMS was confirmed by immunostaining of tissue microarrays (data not shown). Although the high expression of *FGFR4* in most cases of RMS indicates that it may be relevant to the biology of this tumor, it is also expressed in some other cancers³⁷ and normal tissues³⁸. This indicates that although *FGFR4* expression in RMS may be of biological and therapeutic interest, it is unlikely to be applicable as a sole differential diagnostic marker for these tumors.

As the main purpose of this study was to optimize the classification of these cancers, we used a stringent quality filter to include only the genes for which there were good measurements for all samples. This may remove certain genes that are highly expressed in some cancers, but not expressed in other cancers, or may appear not to be expressed because of an artifact in a particular cDNA spot. However, we found that this quality filtration produced more robust prediction models and led to the identification of a set of 96 genes highly relevant to these cancers. Nonetheless, we expect that this list can be expanded by the use of more comprehensive arrays and larger sample sets for training.

Here we developed a method of diagnostic classification of cancers from their gene expression signatures using ANNs. We also identified in ranked order the genes that contributed to this classification, and we were able to define a minimal set that can correctly classify our samples into their diagnostic categories. Although we achieved high sensitivity and specificity for diagnostic classification, we believe that with larger arrays and more samples it will be possible to improve on the sensitivity of these models for purposes of diagnosis in clinical practice. To our knowledge, this is the first application of ANN for diagnostic classification of cancer using gene-expression data derived from cDNA microarrays. Future applications of these methods will include studies to classify cancers according to stage and biological behavior in order to predict prognosis and thereby direct therapy. We believe this offers an alternative and powerful technique for the detection of gene-expression signatures, and the discovery of novel genes that characterize a diagnostic subgroup may also identify new targets for therapy.

Methods

Cell culture and tumor samples

The source and other information for the cell lines and tumor samples used in this study are described in Supplemental Table A (for the training set) and Table 1 (for the test set). All the original histological diagnoses were made at tertiary hospitals, which have reference diagnostic laboratories with extensive experience in the diagnosis of pediatric cancers. Approximately 20% of all samples in each category were randomly selected, blinded and set aside for testing. To augment this test set, we added 4 neuroblastoma tumors and 5 non-SRBCT samples (also blinded to the authors performing the analysis). The EWSs had a spectrum of the expected translocations, and the RMSs were a mixture of both ARMS containing the *PAX3-FKHR* translocation and embryonal rhabdomyosarcoma (ERMS). The NBs contained both *MYCN* amplified and single copy samples. The NHLs were cell lines derived from BL (see Supplemental Table B for details of all samples). The conditions for cell cultures and the methods for extracting RNA from cell lines were described⁵.

Microarray experiments

Preparation of glass cDNA microarrays, probe labeling, hybridization and image acquisition were performed according to the standard NHGRI protocol (<http://www.nhgri.nih.gov/DIR/LCG/15K/HTML/protocol.html>). Image analysis was performed using DeArray software³⁹. The cDNA clones were obtained from Research Genetics (Huntsville, Alabama) and were their standard microarray set, which consisted of 3789 sequence-verified known genes and 2778 sequence-verified ESTs.

Data analysis

We filtered genes by requiring that a gene should have red intensity greater than 20 across all experiments. The number of genes that passed this filter was 2308. Each slide was normalized across all experiments such that the relative (or normalized) red intensity (RRI) for each gene was defined as: $RRI = \text{mean intensity of that spot} / \text{mean intensity of filtered genes}$. The natural logarithm (\ln) of RRI was used as a measure of the expression levels. Hierarchical clustering and MDS plots were performed as described⁵.

To allow for a supervised regression model with no over-training (when we have low number of parameters as compared to the number of samples), the dimensionality of the samples was reduced by PCA (ref. 40) using centralized $\ln(RRI)$ values as input. Thus each sample was represented by 88 numbers, which are the results of projection of the gene expressions using PCA eigenvectors. We used the 10 dominant PCA components for subsequent analysis. We classified the training samples in the 4 categories using a 3-fold cross validation procedure: the 63 training (labeled) samples were randomly shuffled and split into 3 equally sized groups (see Fig. 1a). Each linear ANN model was then calibrated with the 10 PCA input variables (normalized to centralized z-scores) using 2 of the groups, with the third group reserved for testing predictions (validation). This procedure was repeated 3 times, each time with a different group used for validation. The random shuffling was redone 1250 times and for each shuffling we analyzed 3 ANN models. Thus, in total, each sample belonged to a validation set 1250 times, and 3750 ANN models were calibrated. For each diagnostic category (EWS, RMS, NB or BL), each ANN model gave an output between 0 (not this category) and 1 (this category). The 1250 outputs for each validation sample were used as a committee as follows. We calculated the average of all the predicted outputs (a committee vote) and then a sample is classified as a particular cancer if it receives the highest committee vote for that cancer. In clinical settings, it is important to be able to reject a diagnostic classification including samples not belonging to any of the four diagnoses. Therefore, to be able to reject classifications we did as follows. A squared Euclidean distance was computed for each cancer type, between the

committee vote for a sample and the 'ideal' output for that cancer type; normalized such that it is unity between cancer types (see Supplemental Methods). Using the 1250 ANN models for each validation sample we constructed for each cancer type an empirical probability distribution for the distances. Using these distributions, samples are only diagnosed as a specific cancer if they lie within the 95th percentile. All 3750 models were used to classify the additional 25 test samples.

The sensitivity to the different genes is determined by the absolute value of the partial derivative of the output with respect to the gene expressions, averaged over samples and ANN models (see Supplemental Methods). A large sensitivity implies that changing the expression influences the output significantly. In this way the genes can be ranked.

Acknowledgements

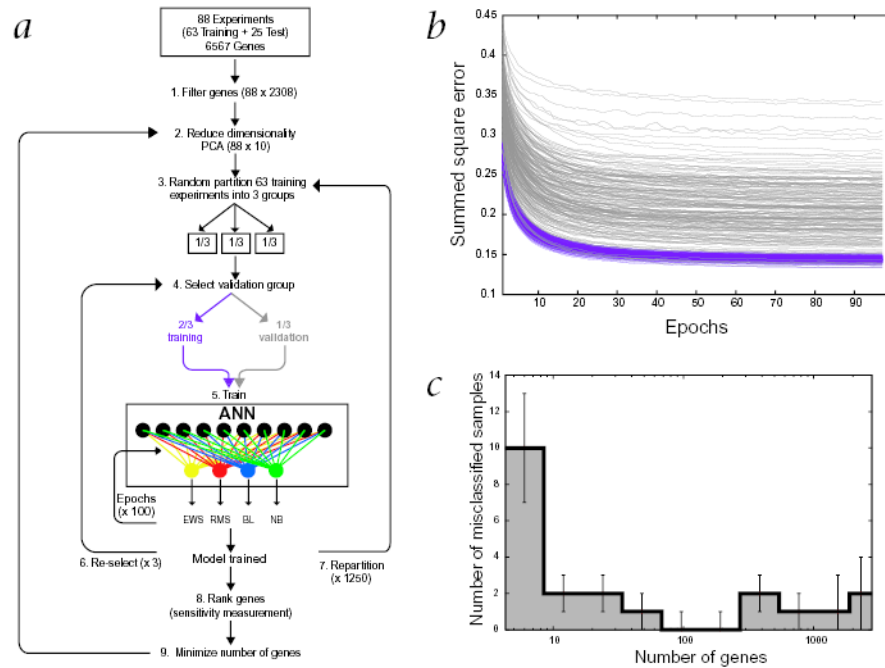
We thank K. Gayton, C. Tsokos, T. Fadiran, J. Lueders and R. Walker for their technical assistance; M. Ohlsson for valuable discussions on ANNs; R. Simon, M. Bittner, Y. Chen and S. Gruberger for their helpful comments regarding the data analysis; and M. Tsokos, L. Helman and C. Thiele for cell lines supplied from the NCI. J.S.W. was in part supported by the Charles & Dana Nearburg Foundation. M.R. was in part supported by the Swedish Research Council and the Knut and Alice Wallenberg Foundation through the SWEGENE consortium. C.P. was in part supported by the Swedish Foundation for Strategic Research.

References

1. Pizzo, P.A. *Principles and practice of pediatric oncology* (Lippincott-Raven, Philadelphia, 1997).
2. Triche TJ, Askin FB. Neuroblastoma and the differential diagnosis of small-, round-, blue- cell tumors. *Hum Pathol* 1983;14:569–595. [PubMed: 6345338]
3. Taylor C, et al. Diagnosis of Ewing's sarcoma and peripheral neuroectodermal tumour based on the detection of t(11;22) using fluorescence *in situ* hybridisation. *Br J Cancer* 1993;67:128–133. [PubMed: 8381297]
4. McManus AP, Gusterson BA, Pinkerton CR, Shipley JM. The molecular pathology of small round-cell tumours—relevance to diagnosis, prognosis, and classification. *J Pathol* 1996;178:116–121. [PubMed: 8683375]
5. Khan J, et al. Gene expression profiling of alveolar rhabdomyosarcoma with cDNA microarrays. *Cancer Res* 1998;58:5009–5013. [PubMed: 9823299]
6. Alizadeh AA, et al. Distinct types of diffuse large B-cell lymphoma identified by gene expression profiling. *Nature* 2000;403:503–511. [PubMed: 10676951]
7. Bittner M, et al. Molecular classification of cutaneous malignant melanoma by gene expression profiling. *Nature* 2000;406:536–540. [PubMed: 10952317]
8. Golub TR, et al. Molecular classification of cancer: class discovery and class prediction by gene expression monitoring. *Science* 1999;286:531–537. [PubMed: 10521349]
9. Bishop, C.M. *Neural Networks for Pattern Recognition* (Clarendon Press, Oxford, 1995).
10. Heden B, Ohlin H, Rittner R, Edenbrandt L. Acute myocardial infarction detected in the 12-lead ECG by artificial neural networks. *Circulation* 1997;96:1798–1802. [PubMed: 9323064]
11. Silipo R, Gori M, Taddei A, Varanini M, Marchesi C. Classification of arrhythmic events in ambulatory electrocardiogram, using artificial neural networks. *Comput Biomed Res* 1995;28:305–318. [PubMed: 8549122]
12. Ashizawa K, et al. Artificial neural networks in chest radiography: application to the differential diagnosis of interstitial lung disease. *Acad Radiol* 1999;6:2–9. [PubMed: 9891146]
13. Abdolmaleki P, et al. Neural network analysis of breast cancer from MRI findings. *Radiat Med* 1997;15:283–293. [PubMed: 9445150]
14. Eisen MB, Spellman PT, Brown PO, Botstein D. Cluster analysis and display of genome-wide expression patterns. *Proc Natl Acad Sci USA* 1998;95:14863–14868. [PubMed: 9843981]
15. deLapeyriere O, et al. Expression of the *Fgf6* gene is restricted to developing skeletal muscle in the mouse embryo. *Development* 1993;118:601–611. [PubMed: 8223280]

16. Jaakkola S, et al. Amplification of fgfr4 gene in human breast and gynecological cancers. *Int J Cancer* 1993;54:378–382. [PubMed: 8099571]
17. Shaoul E, Reich-Slotky R, Berman B, Ron D. Fibroblast growth factor receptors display both common and distinct signaling pathways. *Oncogene* 1995;10:1553–1561. [PubMed: 7731710]
18. Kovar H, et al. Overexpression of the pseudoautosomal gene MIC2 in Ewing's sarcoma and peripheral primitive neuroectodermal tumor. *Oncogene* 1990;5:1067–1070. [PubMed: 1695726]
19. Kumar S, Perlman E, Harris CA, Raffeld M, Tsokos M. Myogenin is a specific marker for rhabdomyosarcoma: an immunohistochemical study in paraffin-embedded tissues. *Mod Pathol* 2000;13:988–993. [PubMed: 11007039]
20. DeRisi J, et al. Use of a cDNA microarray to analyse gene expression patterns in human cancer. *Nature Genet* 1996;14:457–460. [PubMed: 8944026]
21. Perou CM, et al. Molecular portraits of human breast tumours. *Nature* 2000;406:747–752. [PubMed: 10963602]
22. Hedenfalk I, et al. Gene-expression profiles in hereditary breast cancer. *N Engl J Med* 2001;344:539–548. [PubMed: 11207349]
23. Brown MP, et al. Knowledge-based analysis of microarray gene expression data by using support vector machines. *Proc Natl Acad Sci USA* 2000;97:262–267. [PubMed: 10618406]
24. Furey TS, et al. Support vector machine classification and validation of cancer tissue samples using microarray expression data. *Bioinformatics* 2000;16:906–914. [PubMed: 11120680]
25. Mu J, Roach PJ. Characterization of human glycogenin-2, a self-glucosylating initiator of liver glycogen metabolism. *J Biol Chem* 1998;273:34850–34856. [PubMed: 9857012]
26. Lee MG, Loomis C, Cowan NJ. Sequence of an expressed human beta-tubulin gene containing ten Alu family members. *Nucleic Acids Res* 1984;12:5823–5836. [PubMed: 6462917]
27. Savchenko VL, McKanna JA, Nikonenko IR, Skibo GG. Microglia and astrocytes in the adult rat brain: comparative immunocytochemical analysis demonstrates the efficacy of lipocortin 1 immunoreactivity. *Neuroscience* 2000;96:195–203. [PubMed: 10683423]
28. Nagano T, et al. Differentially expressed olfactomedin-related glycoproteins (Pancortins) in the brain. *Brain Res Mol Brain Res* 1998;53:13–23. [PubMed: 9473566]
29. Takahashi Y, Campbell EA, Hirata Y, Takayama T, Listowsky I. A basis for differentiating among the multiple human MUGLUTATHIONE S- transferases and molecular cloning of brain GSTM5. *J Biol Chem* 1993;268:8893–8898. [PubMed: 8473333]
30. Cavazzana AO, Miser JS, Jefferson J, Triche TJ. Experimental evidence for a neural origin of Ewing's sarcoma of bone. *Am J Pathol* 1987;127:507–518. [PubMed: 3035930]
31. McKarney LA, Overall ML, Dziadek M. Myogenesis in cultures of uniparental mouse embryonic stem cells: differing patterns of expression of myogenic regulatory factors. *Int J Dev Biol* 1997;41:485–490. [PubMed: 9240565]
32. Strohman RC, Micou-Eastwood J, Glass CA, Matsuda R. Human fetal muscle and cultured myotubes derived from it contain a fetal-specific myosin light chain. *Science* 1983;221:955–957. [PubMed: 6879193]
33. Song WK, Wang W, Foster RF, Bielser DA, Kaufman SJ. H36-alpha 7 is a novel integrin alpha chain that is developmentally regulated during skeletal myogenesis. *J Cell Biol* 1992;117:643–657. [PubMed: 1315319]
34. Green BN, et al. Distinct expression patterns of insulin-like growth factor binding proteins 2 and 5 during fetal and postnatal development. *Endocrinology* 1994;134:954–962. [PubMed: 7507840]
35. El-Badry OM, et al. Insulin-like growth factor II acts as an autocrine growth and motility factor in human rhabdomyosarcoma tumors. *Cell Growth Differ* 1990;1:325–331. [PubMed: 2177632]
36. Khan J, et al. cDNA microarrays detect activation of a myogenic transcription program by the PAX3-FKHR fusion oncogene. *Proc Natl Acad Sci USA* 1999;96:13264–13269. [PubMed: 10557309]
37. Holtrich U, Brauninger A, Strebhardt K, Rubsamen-Waigmann H. Two additional protein-tyrosine kinases expressed in human lung: fourth member of the fibroblast growth factor receptor family and an intracellular protein-tyrosine kinase. *Proc Natl Acad Sci USA* 1991;88:10411–10415. [PubMed: 1720539]

38. Hughes SE. Differential expression of the fibroblast growth factor receptor (FGFR) multigene family in normal human adult tissues. *J Histochem Cytochem* 1997;45:1005–1019. [PubMed: 9212826]
39. Chen Y, Dougherty ER, Bittner ML. Ratio-based decisions and the quantitative analysis of cDNA microarray images. *Biomedical Optics* 1997;2:364–374.
40. Jolliffe, I.T. *Principal Component Analysis* (Springer, New York, 1986).

**Fig. 1.**

The artificial neural network. **a**, Schematic illustration of the analysis process. The entire dataset of all 88 experiments was first quality filtered (1) and then the dimensionality was further reduced by principal component analysis (PCA) to 10 PCA projections (2), from the original 6567 expression values. Next, the 25 test experiments were set aside and the 63 training experiments were randomly partitioned into 3 groups (3). One of these groups was reserved for validation and the remaining 2 groups for calibration (4). ANN models were then calibrated using for each sample the 10 PCA values as input and the cancer category as output (5). For each model the calibration was optimized with 100 iterative cycles (epochs). This was repeated using each of the 3 groups for validation (6). The samples were again randomly partitioned and the entire training process repeated (7). For each selection of a validation group one model was calibrated, resulting in a total of 3750 trained models. Once the models were calibrated they were used to rank the genes according to their importance for the classification (8). The entire process (2–7) was repeated using only top ranked genes (9). The 25 test experiments were subsequently classified using all the calibrated models. **b**, Monitoring the calibration of the models. The average classification error per sample (using a summed square error function) is plotted during the training iterations (epochs) for both the training and the validation samples. A pair of lines, purple (training) and gray (validation), represents one model. The decrease in the classification errors with increasing epochs demonstrates the learning of the models to distinguish these cancers. The results shown are for 200 different models, each corresponding to a random partitioning of the data. All the models performed well for both training and validation as demonstrated by the parallel decrease (with increasing epochs) of the average summed square classification error per sample. In addition, there was no sign of over-training: if the models begin to learn features in the training set, which are not present in the validation set, this would result in an increase in the error for the validation at that point and the curves would no longer remain parallel. **c**, Minimizing the number of genes. The average number of misclassified samples for all 3750 models is plotted against increasing number of used genes. The misclassifications minimized to zero using the 96 highest ranked genes.

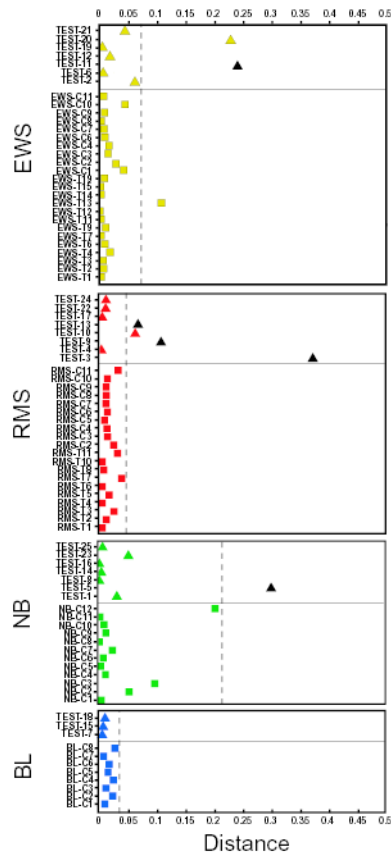


Fig. 2.

Classification and diagnosis of the samples. A sample is classified to a cancer category according to its highest committee vote (average of all ANN outputs) and placed in the corresponding plot. Plotted, for each sample, is the distance from its committee vote to the ideal vote for that diagnostic category (for example, for EWS, it is $EWS = 1$, $RMS = NB = BL = 0$). Thus a perfectly classified sample would be plotted with a distance of zero. Training samples are displayed as squares and test samples as triangles. Non-SRBCT samples are colored black. All SRBCT samples, including the 20 tests, were correctly classified. The distance corresponding to the 95th percentile for the training samples is represented by a dashed line, outside which the diagnosis of a sample is rejected. The diagnosis of all 5 non-SRBCT test samples was rejected since they lie outside their respective dashed lines. Three of the SRBCT samples (EWS-T13, TEST-10 and TEST-20) though correctly classified could not be confidently diagnosed.

Methods), and the ANN rank. *, genes that have not been reported to be associated with these cancers. *c*, Enlargement of the hierarchical clustering dendrogram of the samples in *b*. All 63 training and the 20 test SRBCTs correctly clustered within their diagnostic categories. In both cases where two samples were derived from the same cell line, BL-C2 & C4, and NB-C2 and C7, each mapped adjacent to one another in the same cluster. The scale shows the Pearson correlation coefficient used to construct the dendrogram. The Pearson correlation cutoff was 0.54, when the samples clustered into the four diagnostic categories.

Table 1

ANN diagnostic prediction

Sample label	ANN committee vote				ANN classification	ANN diagnosis	Histological diagnosis	Source label	Source
	EWS	RMS	NB	BL					
Test 1	0.01	0.07	0.76	0.06	NB	NB	NB-C	IMR32	ATCC
Test 2	0.67	0.06	0.08	0.09	EWS	EWS	EWS-C	CHOP1	NCI
Test 3	0.11	0.17	0.16	0.11	RMS	RMS	Osteosarcoma-C	OsA-CI	ATCC
Test 4	0.00	0.95	0.06	0.03	RMS	RMS	ARMS-T	ARMD1	CHTN
Test 5	0.11	0.11	0.25	0.10	NB	NB	Sarcoma-C	A204	ATCC
Test 6	0.98	0.04	0.10	0.03	EWS	EWS	EWS-T	9608P053	CHTN
Test 7	0.05	0.02	0.05	0.93	BL	BL	BL-C	EB1	ATCC
Test 8	0.00	0.05	0.94	0.04	NB	NB	NB-C	SMSSAN	NCI
Test 9	0.22	0.60	0.03	0.06	RMS	RMS	Sk. Muscle	SKM1	CHTN
Test 10	0.10	0.68	0.11	0.04	RMS	RMS	ERMS-T	ERDM1	CHTN
Test 11	0.39	0.04	0.28	0.15	EWS	EWS	Prostate Ca.-C	PC3	ATCC
Test 12	0.89	0.05	0.14	0.03	EWS	EWS	EWS-T	SARG67	CHTN
Test 13	0.20	0.7	0.03	0.05	RMS	RMS	Sk. Muscle	SKM2	CHTN
Test 14	0.03	0.02	0.90	0.07	NB	NB	NB-T	NB3	DZNSG
Test 15	0.06	0.03	0.05	0.91	BL	BL	BL-C	EB2	ATCC
Test 16	0.03	0.02	0.93	0.05	NB	NB	NB-T	NB1	DZNSG
Test 17	0.01	0.90	0.03	0.03	RMS	RMS	ARMS-T	ARMD2	CHTN
Test 18	0.06	0.04	0.04	0.88	BL	BL	BL-C	GA10	ATCC
Test 19	0.99	0.02	0.02	0.04	EWS	EWS	EWS-T	ET3	CHTN
Test 20	0.40	0.30	0.10	0.06	EWS	EWS	EWS-T	9903P1339	CHTN
Test 21	0.81	0.19	0.12	0.04	EWS	EWS	EWS-T	ES23	MSKCC
Test 22	0.01	0.88	0.09	0.04	RMS	RMS	ERMS-T	ERMD2	CHTN
Test 23	0.07	0.08	0.70	0.06	NB	NB	NB-T	NB2	DZNSG
Test 24	0.05	0.87	0.06	0.03	RMS	RMS	ERMS-T	RMS4	MSKCC
Test 25	0.05	0.02	0.89	0.06	NB	NB	NB-T	NB4	DZNSG

Source label refers to the original name of the sample as designated by the source. Histological diagnosis is defined as cancer type suffixed with -T for a tumor sample and -C for a cell line. Normal skeletal muscle (Sk. Muscle) is also included in the test set. The ANN classification as determined by the committee vote is bolded. NCI: National Cancer Institute, National Institutes of Health, ATCC: American Type Culture Collection, MSKCC: Memorial Sloan-Kettering Cancer Center, CHTN: Cooperative Human Tissue Network, DZNSG: German Cancer Research Center, Heidelberg.